HHS Public Access

Author manuscript

*ACS Nano*. Author manuscript; available in PMC 2017 August 23.

Published in final edited form as:

*ACS Nano*. 2017 January 24; 11(1): 613–620. doi:10.1021/acsnano.6b06892.

# $H_2O_2$-Responsive Vesicles Integrated with Transcutaneous Patches for Glucose-Mediated Insulin Delivery

**Xiuli Hu**[†,‡], **Jicheng Yu**[†], **Chenggen Qian**[†], **Yue Lu**[†], **Anna R. Kahkoska**[§], **Zhigang Xie**[‡], **Xiabin Jing**[‡], **John B. Buse**[§], and **Zhen Gu**[†,§,*]

[†]Joint Department of Biomedical Engineering, University of North Carolina at Chapel Hill and North Carolina State University, Raleigh, North Carolina 27695, United States

[‡]State Key Laboratory of Polymer Chemistry and Physics, Changchun Institute of Applied Chemistry, Chinese Academy of Sciences, Jilin, 130022, People's Republic of China

[§]Department of Medicine, University of North Carolina School of Medicine, Chapel Hill, North Carolina 27599, United States

## Abstract

A self-regulated "smart" insulin administration system would be highly desirable for diabetes management. Here, a glucose-responsive insulin delivery device, which integrates $H_2O_2$-responsive polymeric vesicles (PVs) with a transcutaneous microneedle-array patch was prepared to achieve a fast response, excellent biocompatibility, and painless administration. The PVs are self-assembled from block copolymer incorporated with polyethylene glycol (PEG) and phenylboronic ester (PBE)-conjugated polyserine (designated mPEG-*b*-P(Ser-PBE)) and loaded with glucose oxidase (GOx) and insulin. The polymeric vesicles function as both moieties of the glucose sensing element (GOx) and the insulin release actuator to provide basal insulin release as well as promote insulin release in response to hyperglycemic states. In the current study, insulin release responds quickly to elevated glucose and its kinetics can be modulated by adjusting the concentration of GOx loaded into the microneedles. *In vivo* testing indicates that a single patch can regulate glucose levels effectively with reduced risk of hypoglycemia.

## Graphical Abstract

[*]Corresponding Author: zgu@email.unc.edu.

**ORCID**

Zhigang Xie: 0000-0003-2974-1825

Zhen Gu: 0000-0003-2947-4456

**Notes**

The authors declare no competing financial interest.

Supporting Information

The Supporting Information is available free of charge on the ACS Publications website at DOI: 10.1021/acsnano.6b06892. Details of materials used; methods for synthesis and characterizations of acrylate modified HA, preparation of cross-linked microneedle, mechanical strength test, *in vitro* insulin release studies, biocompatibility analysis, statistical analysis; additional figures (PDF)

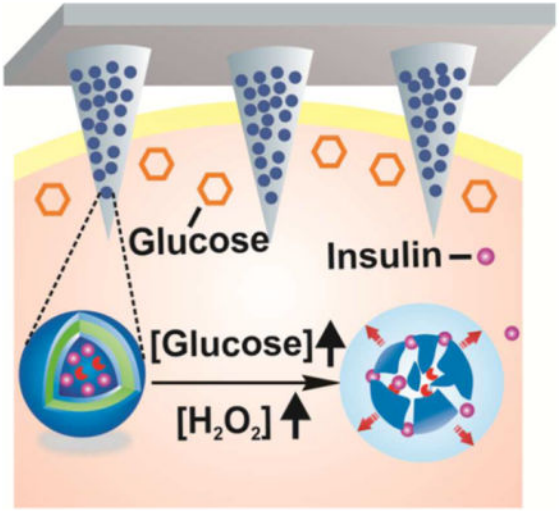


**Keywords**

drug delivery; vesicles; polymersome; glucose-responsive; insulin; diabetes

Diabetes mellitus is a chronic metabolic disorder characterized by elevated blood glucose levels.[1,2] It has become one of the most challenging global health issues and the number of people living with diabetes has increased dramatically.[3,4] Traditional care for type 1 and advanced type 2 diabetic patients requires frequent or constant monitoring of glycemic levels combined with frequent subcutaneous injections of long- and short-acting insulin or using continuous and variable insulin infusions toward the goal of maintaining normoglycemia.[5] Nevertheless, such “open-loop” self-administration of insulin is always painful and generally associated with inadequate glucose control.[6,7]

An alternative to these traditional, open-loop methods of insulin delivery is the use of a closed-loop insulin pump integrated with a continuous glucose monitor.[8] This closed-loop principle has been proven to be efficient in blood glucose control and reducing the risk of hypoglycemia.[9,10] However, there are still several obstacles to overcome regarding the accuracy of the continuous glucose monitor and reliability of insulin infusions.[11,12] Further, the current systems require tubing and subcutaneous implantation of a cannula which is inconvenient and often is associated with biofouling.

Meanwhile, synthetic glucose-responsive materials have been widely explored for achieving closed-loop insulin release, offering the potential of insulin delivery without these limitations.[13] The matrix typically employs glucose-responsive moieties such as glucose oxidase (GOx),[14–18] phenylboronic acid (PBA),[19–23] or glucose binding proteins (GBP)[24,25] to regulate the release rate of the preloaded insulin by polymer degradation, structure switch, or glucose binding competition. However, there remains a challenge to demonstrate a desirable system, which combines (i) ease of use, (ii) high drug loading capacity, (iii) fast responsiveness, and (iv) excellent bio-compatibility. For example, most glucose-responsive

formulations that incorporated GOx involve pH-sensitive materials, based on the enzymatic oxidation of glucose to gluconic acid.

However, these systems are limited because of the challenge of rapidly switching the physiological pH *in vivo*.[2] To this end, we have previously developed a hypoxia-sensitive formulation to achieve fast response.[26] However, hydrogen peroxide ($H_2O_2$) remains in this system, which raises the concern of long-term biocompatibility.[27]

Herein, we describe a glucose-responsive mechanism directly utilizing $H_2O_2$-sensitive[28–34] polymeric vesicles (PVs) for smart insulin delivery (Figure 1). PVs, also known as polymersomes, are usually self-assembled from amphiphilic block copolymers to form hollow structures consisting of an aqueous core and a polymer bilayer membrane.[35–39] They hold great promise for controlled drug delivery due to their robust structures and large loading capacity of hydrophilic molecules.[40–43] Here, the PVs are self-assembled from block copolymer incorporated with polyethylene glycol (PEG) and phenylboronic ester (PBE)-conjugated polyserine (designated mPEG-*b*-P(Ser-PBE)) and have hollow spherical structures with GOx and insulin encapsulated in the interior. The pendant PBE was selected for its facile $H_2O_2$-mediated degradation at physiological conditions[28,44] (Figure 1A and 1B). For the *in vivo* application, these vesicles were further integrated with a transcutaneous microneedle-array patch. Microneedles, which typically have a needle length shorter than one millimeter, have become an attractive transdermal drug delivery technology due to easy use and improved patient compliance.[45–50] Cross-linked hyaluronic acid (HA) was chosen to prepare the microneedles in order to achieve excellent biocompatibility and sufficient stiffness.[51] When the microneedle patch was applied to diabetic mice, as shown in Figure 1C, glucose can diffuse across the membrane and interact with GOx in the cavity, which leads to the oxidation of glucose to gluconic acid, simultaneously generating $H_2O_2$:[26]

$$\text{glucose} + O_2 + H_2O \xrightarrow{\text{GOx}} \text{gluconic acid} + H_2O_2$$

By virtue of the generated $H_2O_2$, the copolymer mPEG-*b*-P(Ser-PBE) loses its PBE side chains and becomes water-soluble, leading to disassemble of the PVs and subsequent release of the preloaded insulin.[28] The final transcutaneous device was expected to provide a desirable smart insulin delivery system with high drug loading capacity, fast response, and painless administration.

## RESULTS AND DISCUSSION

### Synthesis and Characterization of Polymer Vesicles (PVs)

The diblock copolymer (mPEG-*b*-polyserine) was first synthesized via the amine-initiated ring-opening polymerization (ROP) of *N*-carboxy-*α*-amino acid anhydrides (NCA) of serine.[52–54] 4-(Hydroxymethyl)phenylboronic acid pinacol ester (PBE) was then conjugated to the pendant hydroxyl groups of the serine residue via a carbonate linkage (Figure 1A and Figure S1). The polymerization degree of the polyserine block was calculated to be 60, after which 75% of its hydroxyl groups were conjugated with PBE, determined by using the $^1H$ NMR peak area with the methylene peak of mPEG as a standard (Figure S2). The

hydrophobic PBE groups have two main functions: (1) to change the solubility of the polymer and enable the formation of PVs in the aqueous solution, and (2) to provide facile $H_2O_2$-mediated dissociation of PVs (Figure 1A), and rapid release of GOx and insulin.

Self-assembly of the obtained diblock copolymer mPEG-*b*-P(Ser-PBE) was conducted using a solvent evaporation method. The morphology was characterized by transmission electron microscopy (TEM) and dynamic light scatting (DLS). As shown in Figure 2A, the TEM image indicated that spherical PVs with hollow structures were obtained. The average diameter of the obtained PVs was determined as 200 nm by DLS (Figure 2B). The stability of the obtained PVs was confirmed by DLS and no significant diameter change was observed for over 1 week at 4 °C (Figure S3). The PVs were then used to encapsulate insulin and GOx enzyme. As shown in the TEM image (Figure 2A), after encapsulating insulin and GOx, the cavity of the PVs(E+I) was filled, and the average diameter increased to 220 nm, determined by DLS (Figure 2B), which was consistent with the result from TEM (Figure 2A). The zeta-potentials of PVs and PVs(E+I) were measured to be −14.4 and −14.1 mV, respectively. In the fluorescence image of PVs, FITC-labeled insulin was used to be loaded into the PVs, and the spiculate cluster shown in Figure 2C represented the PVs, confirming the successful encapsulation of insulin. The insulin loading content of PVs was determined as 12.5 ± 0.5% (w/w), and the loading efficiency was determined as 82.5 ± 1.0%.

The $H_2O_2$-responsive capability of insulin loaded vesicles was tested by incubating the vesicles in PBS buffer with different $H_2O_2$ concentrations (0, 50, 200 $\mu$M). An increased insulin release profile was observed with increase of $H_2O_2$ concentration as shown in Figure S4. Following, the $H_2O_2$-responsive disassembly of PVs mediated by glucose was examined by incubating the vesicles in PBS buffer at a glucose concentration of 400 mg/dL, a typical hyperglycemic level, and observing the corresponding evolution of size changes. As demonstrated in Figure 2C, the fluorescence signal showed spiculate cluster signal at first, turned to be swelling clusters after 1 h of incubation in glucose solution, and became more homogeneous after 2 h of incubation in glucose solution, verifying the disassembly of the PVs and subsequent FITC-insulin release. The morphology changes of the PVs were also observed in TEM images and DLS (Figure 2D,E). After incubation in glucose solution for 1 h, the PV structures were dissociated and some PVs were recombined into large and small particles. After incubation in glucose solution for 2 h, both vesicle density (population per unit area) and size were further reduced and a large amount of cargo leakage was observed (Figure 2D).

### *In Vitro* Glucose-Responsive Insulin Release

We next assessed the *in vitro* insulin release profile of the vesicles in response to different glucose levels by incubating the vesicles with PBS containing various concentrations of glucose, including a control level (0 mg/dL), a normoglycemic level (100 mg/dL), and a typical hyperglycemic level (400 mg/dL). A significantly rapid insulin release rate was observed at the hyperglycemic level, while limited insulin release was observed at the normoglycemic and control level, as shown in Figure 3A. This release profile was consistent with the above-mentioned dissociation response. When the glucose concentration was increased in steps (100–200–400 mg/dL, 1 h each, Figure 3B), the release rate of insulin

(slope of the lines), increased correspondingly, indicating the responsiveness of insulin release to glucose concentration. When the concentration of glucose varied periodically between 100 and 400 mg/dL for 10 min each time (Figure 3C), a pulsatile release pattern was observed, indicating the rapid response to the change in glucose concentration. Furthermore, when the GOx content in the PVs was reduced to a half (PV($^1/_2$E+I) vs PV(E +I) (Figure 3B), the release rate of insulin decreased correspondingly, implying the possibility of adjusting the insulin release rate by varying the GOx amount in PVs. Additionally, the released insulin has identical secondary structure to that of the native insulin as shown in Figure 3D. Collectively, these results verified that the release of insulin from the PVs was in a glucose-responsive manner with fast responsiveness.

## Fabrication and Characterization of PVs-Loaded Microneedle (MN) Patch

To achieve convenient and painless administration, insulin-loaded PVs were further deposited in the tips of cross-linked hyaluronic acid (HA)-based MN array patch using a micromolding approach.[26] The resulted MN was arranged in a 20 × 20 array with 600 $\mu$m tipto-tip spacing in a 100 mm$^2$ patch as shown in Figure 4A and Figure S5(A). The fluorescence image in Figure 4A(a) represents MNs integrated with FITC-insulin-loaded PVs, indicating PVs were well distributed in the tip region of each needle. The obtained MNs were administered on the back of the mice as shown in Figure 1C and could penetrate into the mouse skin conveniently, as evidenced by the trypan blue staining (Figure 4A(c)) and hematoxylin and eosin stain (H&E) staining (Figure S5(B)). The mechanical strength of MN was measured to be 3 N/needle using a tensile compression machine, which was sufficient to insert into the skin without tip breaking (Figure S6).[51]

To evaluate the biocompatibility of the system, the cytotoxicity of PVs toward HeLa cells was investigated at different concentrations of PVs ranging from 0.1 to 1.0 mg/mL using 3-(4,5)-dimethylthiahiazo(-*z*-*y*1)-3,5-diphenytetra-zoliumromide (MTT) assay. Insignificant toxicity of PVs was observed at any of the concentrations studied (Figure S7). In the *in vivo* assessment of the patch, no significant inflammation was observed in the region 2 d post-administration compared to the surrounding tissue, indicating good biocompatibility of the patch materials (Figure S8). In addition, the microchannels on the skin that were created by insertion of the MN recovered within 6 h post-administration (Figure S9).

## *In Vivo* Studies of the MNs for Type 1 Diabetes Treatment

We then administered the MN-array patch on streptozotocin (STZ)-induced type 1 diabetic mice to evaluate its *in vivo* performance for type 1 diabetes treatment. The mice were randomly divided into four groups and transcutaneously treated with different MN samples, including: 1) the empty MNs containing only cross-linked HA (MN[HA]); 2) MNs loaded with insulin (MN[I]); 3) MNs loaded with PVs encapsulating only insulin (MN[PV(I)]); and 4) MNs loaded with PVs encapsulating GOx enzyme and insulin (MN[PV(E +I)]), with equivalent insulin dose of 10 mg/kg for each mouse. Afterward, the plasma glucose levels of treated mice in each group were monitored over time.

As shown in Figure 4B, the blood glucose in mice treated with MN[I] and MN[PV(E+I)] rapidly decreased to around 90 mg/dL within 1 h. The MN[I] group quickly lost control over

the subsequent hour. The MN[PV(E+I)] group remained in the normoglycemic range (<200 mg/dL) for ~5 h with a subsequent gradual increase in blood glucose levels. The control and MN[PV(I)] group animals showed insignificant decreases in glucose, indicating the requirement for GOx in the PVs *in vivo* for adequate PV disassembly and insulin release. An enzyme-linked immunosorbent assay (ELISA) was used to quantify insulin in the plasma of treated mice. As shown in Figure 4C, mice treated with MN[PV(E+I)] kept a consistently higher plasma insulin level than those administered with MN[PV(I)] for at least 24 h, indicating again the role of loaded GOx in the PVs dissociation and insulin release, in support to the *in vitro* result in Figure 3B.

Following, a glucose tolerance test was conducted via intraperitoneally (i.p.) injecting glucose solutions of 1.5 g/kg in diabetic mice 1 h after administration of MN[PV(E+I)] and MN[I]. Healthy mice were injected with glucose solution without administration of microneedle patches. As shown in Figure 4D, 1 h after administration of MNs, the two groups of diabetic mice had similar starting glucose levels as the untreated healthy mice. After an i.p. injection of glucose, blood glucose levels of the three groups increased steadily and reached their peaks (268, 330, and 470 mg/dL) at 20, 30, and 50 min, respectively. Then glucose levels declined gradually. After about 120 min, the MN[PV(E+I)] animals were back to normogly-cemic range (<200 mg/dL), while in the MN[I] group glucose levels remained around 400 mg/dL. To quantify the glucose response to i.p. glucose injection, the area under the blood glucose level curve between 0 and 150 min was calculated for each group. As shown in Figure 4E, the MN[PV(E+I)] treated mice showed significantly improved resistance to the glucose challenge compared to those treated with MN[I]. Finally, to evaluate the hypoglycemic potential of the patches, MN[PV(E+I)], MN[PV(I)], and MN[I] were applied to healthy mice. As shown in Figure 4F, a remarkable decrease in glucose was observed in mice treated with MN[I], while there was little change in mice treated with MN[PV(E+I)] or MN[PV(I)], indicating negligible insulin leakage from MN[PV(E+I)] and MN[PV(I)] and reduced risk of hypoglycemia compared with MN[I]. To quantify these differences and evaluate the risk of hypoglycemia, the hypoglycemia index was calculated (Figure 4G),[22,26] PV-loaded MNs demonstrated a lower hypoglycemic index compared to insulin-loaded MN.

## CONCLUSIONS

In summary, we report a closed-loop, glucose-responsive insulin delivery platform by integrating $H_2O_2$-responsive polymeric vesicles with a painless transcutaneous MN array patch. Utilizing polymeric vesicles, water-soluble insulin was encapsulated into the inner cavity with a high capacity. This formulation demonstrated both *in vitro* and *in vivo* glucose-mediated disassembly, releasing the encapsulated insulin under the hyperglycemic condition with rapid responsiveness. Importantly, when the glucose levels reached the normoglyce-mic state, the release rate of insulin declined, which could avoid the risk of hypoglycemia. As such, the prepared insulin patch provides a clinical opportunity for closed-loop insulin delivery with its special trigger mechanism to mimic the function of pancreatic beta-cells to release insulin in a glucose-responsive fashion. Furthermore, this $H_2O_2$-responsive artificial vesicle can be applied as a useful platform for delivering various therapeutics to treat other diseases.[55]

# METHODS

## Synthesis of Boronic Esters Functionalized Block Copolymer

4-(Imidazoyl carbamate)phenylboronic acid pinacol ester (1) was prepared according to the literature.[28] Briefly, 4-(Hydroxymethyl)-phenylboronic acid pinacol ester (PAPE) (4g, 17.1 mmol) was dissolved in dry dichloromethane ($CH_2Cl_2$) (20 mL) in a dried 200 mL flask. Carbonyldiimidazole (5.54 g, 34.2 mmol) was then added to the solution and stirred for 1 h. The mixture was concentrated under vacuum, redissolved in ethyl acetate (200 mL) and washed with $H_2O$ (3 × 10 mL). The organics were dried with $MgSO_4$, and concentrated using a rotary evaporator to give a pure white solid 1 (3.90 g, yield: 70.0%). **1**: $^1$HNMR (400 MHz, CDCl3) $\delta$1.33 (s, 12 H), 5.42 (s, 2 H), 7.05 (s, 1H), 7.43 (m, 3H), 7.85 (d, 2H), 8.14 (s, 1H).

$mPEG_{44}$-*b*-$polyserine_{60}$ (1.0 g, 7.5 mmol OH) was first synthesized according to the literature[52] and then dissolved in anhydrous $CH_2Cl_2$ (20 mL) in a 50 mL of flask. 4-(Imidazoyl carbamate)phenylboronic acid pinacol ester (2.5 g, 7.5 mmol) was added followed by DMAP (0.9 g, 7.5 mmol) addition, and the mixture solution was stirred overnight at room temperature. The product mPEG-*b*-P(Ser-PBE) was obtained by precipitation in cold diethyl ether and dried *in vacuo*.

## Preparation of Polymeric Vesicles

Polymeric vesicles (PVs) were prepared by the solvent evaporation method. Briefly, 40 mg of mPEG-*b*-P(Ser-PBE) was dissolved in 5 mL of THF, followed by injection of 10 mL of DI water with or without 7.5 mg of human insulin and 0.75 mg of GOx dissolved in it. The mixture was stirred at room temperature for 30 min, and then THF was removed by bubbling with $N_2$. The unloaded insulin was removed by centrifugation at 4000*g* for 10 min with a centrifugal filter (25 000 Da molecular mass cutoff, Millipore) and washed with PBS buffer for several times. The obtained PVs suspension was stored at 4 °C for further studies. The loading content and loading efficiency of insulin was tested using a Coomassie Plus protein assay. The absorbance was detected at 595 nm on the Infinite 200 PRO multimode plate reader (Tecan Group Ltd., Switzerland) and the concentration was interpolated from an insulin standard curve. The size distribution and zeta-potential of the PVs were measured using the Zeta sizer (Nano ZS; Malvern). The TEM images were acquired using a JEOL 2000FX TEM.

## *In Vitro* Insulin Release Studies

An 8 mg sample of polymeric vesicles was added to PBS (1 mL) with different glucose concentrations, including 0, 100, or 400 mg/dL, and incubated at 37 °C on an orbital shaker to study the *in vitro* release behavior of insulin. At predetermined time points, 50 $\mu$L of the sample was taken out for analysis and 50 $\mu$L of fresh media was refilled into the tube. Insulin content in the withdrawn sample was determined by absorbance measurement at 595 nm and by virtue of the insulin standard curve. To access the responsiveness of PVs to changes in glucose levels, PVs were incubated in glucose concentrations varied between 100 and 400 mg/dL periodically for 10 min each. The cycle was repeated several times, and the released amount of insulin was measured.

### *In Vivo* Studies Using STZ-Induced Diabetic Mice

The *in vivo* performance of the prepared MN-array patches was assessed on STZ-induced adult diabetic mice (male C57B6, 20–25 g, Jackson Lab) for diabetes management. The animal study protocol was approved by the Institutional Animal Care and Use Committee at North Carolina State University and University of North Carolina at Chapel Hill. The mice were divided into four groups randomly with five mice for each group and transcutaneously treated with empty MN containing only m-HA, MN loaded with insulin MN[I], MN loaded with PVs encapsulating insulin and enzyme MN[PV(E+I)], or MN loaded with PVs encapsulating only insulin MN[PV(I)], respectively. The insulin dose was 10 mg/kg for each mouse. The plasma glucose levels of the mice in each group were monitored over time (at 10, 20, 40, and 60 min, and once per hour afterward) by collecting blood samples (~3 μL) from the tail vein and determined using the Clarity GL2Plus glucose meter (Clarity Diagnostics, Boca Raton, Florida) until a return to stable hyperglycemia. To measure the plasma insulin concentration *in vivo*, blood samples (25 μL) were collected from the tail vein. The serum was isolated and stored at −20 °C for plasma insulin assay using Human Insulin ELISA kit according to the manufacturer's protocol (Calbiotech, U.S.A.). A intraperitoneal glucose tolerance test (IPGTT) was conducted to verify the *in vivo* glucose responsiveness of MNs 1 h post-administration of MNs. Briefly, mice were administrated with MN[PV(E+I)] and MN[I] (the insulin dose is 10 mg/kg for each mouse), and then a glucose solution in PBS buffer was intra-peritoneally injected with glucose dose of 1.5 g/kg for each mouse and the blood glucose levels were monitored over time. The side effects of MNs were evaluated on healthy mice by administration with MN[PV(E+I)], MN[PV(I)], and MN[I].

### Statistics

All data presented are Mean ± s.d. Statistical analysis was performed using Student's *t* test. The differences between experimental groups and control groups were considered statistically significant for $P$ value <0.05.

## Supplementary Material

Refer to Web version on PubMed Central for supplementary material.

## Acknowledgments

This work was supported by the grants from the American Diabetes Association (ADA) to Z.G. (1-15-ACE-21) and the grant from NC TraCS, NIH's Clinical and Translational Science Awards (CTSA, NIH Grant 1UL1TR001111) at UNC-CH, and the National Science Foundation (NSF) through the ASSIST Engineering Research Center at NC State (EEC-1160483).

## References

1. Stumvoll M, Goldstein BJ, van Haeften TW. Type 2 Diabetes: Principles of Athogenesis and Therapy. Lancet. 2005; 365:1333–1346.
2. Mo R, Jiang T, Di J, Tai W, Gu Z. Emerging Micro- and Nanotechnology Based Synthetic Approaches for Insulin Delivery. Chem Soc Rev. 2014; 43:3595–3629. [PubMed: 24626293]
3. Shaw JE, Sicree RA, Zimmet PZ. Global Estimates of the Prevalence of Diabetes for 2010 and 2030. Diabetes Res Clin Pract. 2010; 87:4–14. [PubMed: 19896746]

4. Wild S, Roglic G, Green A, Sicree R, King H. Global Prevalence of Diabetes Estimates for the Year 2000 and Projections for 2030. Diabetes Care. 2004; 27:1047–1053. [PubMed: 15111519]
5. Raskin P, Allen E, Hollander P, Lewin A, Gabbay RA, Hu P, Bode B, Garber A. Initiating Insulin Therapy in Type 2 Diabetes A comparison of Biphasic and Basal Insulin Analogs. Diabetes Care. 2005; 28:260–265. [PubMed: 15677776]
6. Jeandidier N, Boivin S. Current Status and Future Prospects of Parenteral Insulin Regimens, Strategies and Delivery Systems for Diabetes Treatment. Adv Drug Delivery Rev. 1999; 35:179–198.
7. Veiseh O, Tang BC, Whitehead KA, Anderson DG, Langer R. Managing Diabetes with Nanomedicine: Challenges and Opportunities. Nat Rev Drug Discovery. 2015; 14:45–57. [PubMed: 25430866]
8. Thabit H, Hovorka R, Evans M. Artificial Pancreas: The Bridge to a Cure for Type 1 Diabetes. Eur Diab Nursing. 2012; 9:56–60.
9. Choudhary P, Shin J, Wang Y, Evans ML, Hammond PJ, Kerr D, Shaw JA, Pickup JC, Amiel SA. Insulin Pump Therapy with Automated Insulin Suspension in Response to Hypoglycemia Reduction in Nocturnal Hypoglycemia in Those at Greatest Risk. Diabetes Care. 2011; 34:2023–2025. [PubMed: 21868778]
10. Russell SJ, El-Khatib FH, Sinha M, Magyar KL, McKeon K, Goergen LG, Balliro C, Hillard MA, Nathan DM, Damiano ER. Outpatient Glycemic Control with a Bionic Pancreas In Type 1 Diabetes. N Engl J Med. 2014; 371:313–325. [PubMed: 24931572]
11. Bratlie KM, York RL, Invernale MA, Langer R, Anderson DG. Materials for Diabetes Therapeutics. Adv Healthcare Mater. 2012; 1:267–284.
12. Stevenson CL, Santini JT, Langer R. Reservoir-Based Drug Delivery Systems Utilizing Microtechnology. Adv Drug Delivery Rev. 2012; 64:1590–1602.
13. Wu Q, Wang L, Yu H, Wang J, Chen Z. Organization of Glucose-Responsive Systems and Their Properties. Chem Rev. 2011; 111:7855–7875. [PubMed: 21902252]
14. Gu Z, Dang TT, Ma M, Tang BC, Cheng H, Jiang S, Dong Y, Zhang Y, Anderson DG. Glucose-Responsive Microgels Integrated with Enzyme Nanocapsules for Closed-Loop Insulin Delivery. ACS Nano. 2013; 7:6758–6766. [PubMed: 23834678]
15. Podual K, Doyle FJ, Peppas NA. Glucose-Sensitivity of Glucose Oxidase-Containing Cationic Copolymer Hydrogels Having Poly (ethylene glycol) Grafts. J Controlled Release. 2000; 67:9–17.
16. Podual K, Doyle F, Peppas N. Preparation and Dynamic Response of Cationic Copolymer Hydrogels Containing Glucose Oxidase. Polymer. 2000; 41:3975–3983.
17. Napoli A, Boerakker MJ, Tirelli N, Nolte RJ, Sommerdijk NA, Hubbell JA. Glucose-Oxidase Based Self-Destructing Polymeric Vesicles. Langmuir. 2004; 20:3487–3491. [PubMed: 15875368]
18. Gordijo CR, Shuhendler AJ, Wu XY. Glucose-Responsive Bioinorganic Nanohybrid Membrane for Self-Regulated Insulin Release. Adv Funct Mater. 2010; 20:1404–1412.
19. Ma R, Shi L. Phenylboronic Acid-Based Glucose-Responsive Polymeric Nanoparticles: Synthesis and Applications in Drug Delivery. Polym Chem. 2014; 5:1503–1518.
20. Matsumoto A, Ishii T, Nishida J, Matsumoto H, Kataoka K, Miyahara Y. Synthetic Approach Toward a Self-Regulated Insulin Delivery System. Angew Chem, Int Ed. 2012; 51:2124–2128.
21. Kitano S, Koyama Y, Kataoka K, Okano T, Sakurai Y. A Novel Drug Delivery System Utilizing a Glucose Responsive Polymer Complex Between Poly (vinyl alcohol) and Poly (n-vinyl-2-pyrrolidone) with a Phenylboronic Acid Moiety. J Controlled Release. 1992; 19:161–170.
22. Chou DHC, Webber MJ, Tang BC, Lin AB, Thapa LS, Deng D, Truong JV, Cortinas AB, Langer R, Anderson DG. Glucose-Responsive Insulin Activity by Covalent Modification with Aliphatic Phenylboronic Acid Conjugates. Proc Natl Acad Sci U S A. 2015; 112:2401–2406. [PubMed: 25675515]
23. Kim H, Kang YJ, Kang S, Kim KT. Monosaccharide-Responsive Release of Insulin from Polymersomes of Polyboroxole Block Copolymers at Neutral pH. J Am Chem Soc. 2012; 134:4030–4033. [PubMed: 22339262]
24. Brownlee M, Cerami A. A Glucose-Controlled Insulin-Delivery System: Semisynthetic Insulin Bound to Lectin. Science. 1979; 206:1190–1191. [PubMed: 505005]

25. Kim SW, Paii CM, Kimiko M, Seminoff LA, Holmberg DL, Gleeson JM, Wilson DE, Mack EJ. Self-Regulated Glycosylated Insulin Delivery. J Controlled Release. 1990; 11:193–201.
26. Yu J, Zhang Y, Ye Y, DiSanto R, Sun W, Ranson D, Ligler FS, Buse JB, Gu Z. Microneedle-Array Patches Loaded with Hypoxia-Sensitive Vesicles Provide Fast Glucose-Responsive Insulin Delivery. Proc Natl Acad Sci U S A. 2015; 112:8260–8265. [PubMed: 26100900]
27. Saravanakumar G, Kim J, Kim WJ. Reactive-Oxygen-Species-Responsive Drug Delivery Systems: Promises and Challenges. Adv Sci. 2016:1600124.
28. Broaders KE, Grandhe S, Fréchet JM. A Biocompatible Oxidation-Triggered Carrier Polymer with Potential in Therapeutics. J Am Chem Soc. 2010; 133:756–758.
29. Joshi-Barr S, de Gracia Lux C, Mahmoud E, Almutairi A. Exploiting Oxidative Microenvironments in The Body as Triggers for Drug Delivery Systems. Antioxid Redox Signaling. 2014; 21:730–754.
30. Mahmoud EA, Sankaranarayanan J, Morachis JM, Kim G, Almutairi A. Inflammation Responsive Logic Gate Nanoparticles for The Delivery of Proteins. Bioconjugate Chem. 2011; 22:1416–1421.
31. Napoli A, Valentini M, Tirelli N, Müller M, Hubbell JA. Oxidation-Responsive Polymeric Vesicles. Nat Mater. 2004; 3:183–189. [PubMed: 14991021]
32. Wilson DS, Dalmasso G, Wang L, Sitaraman SV, Merlin D, Murthy N. Rally Delivered Thioketal Nanoparticles Loaded with TNF-A-Sirna Target Inflammation and Inhibit Gene Expression in The Intestines. Nat Mater. 2010; 9:923–928. [PubMed: 20935658]
33. Lee SH, Gupta MK, Bang JB, Bae H, Sung HJ. Current Progress in Reactive Oxygen Species (ROS)-Responsive Materials for Biomedical Applications. Adv Healthcare Mater. 2013; 2:908–915.
34. Liu X, Xiang J, Zhu D, Jiang L, Zhou Z, Tang J, Liu X, Huang Y, Shen Y. Fusogenic Reactive Oxygen Species Triggered Charge-Reversal Vector for Effective Gene Delivery. Adv Mater. 2016; 28:1743–1752. [PubMed: 26663349]
35. Tanner P, Baumann P, Enea R, Onaca O, Palivan C, Meier W. Polymeric Vesicles: from Drug Carriers to Nanoreactors and Artificial Organelles. Acc Chem Res. 2011; 44:1039–1049. [PubMed: 21608994]
36. Discher DE, Eisenberg A. Polymer Vesicles. Science. 2002; 297:967–973. [PubMed: 12169723]
37. Mai Y, Eisenberg A. Self-Assembly of Block Copolymers. Chem Soc Rev. 2012; 41:5969–5985. [PubMed: 22776960]
38. Palivan CG, Goers R, Najer A, Zhang X, Car A, Meier W. Bioinspired Polymer Vesicles and Membranes for Biological and Medical Applications. Chem Soc Rev. 2016; 45:377–411. [PubMed: 26563574]
39. Städler B, Price AD, Zelikin AN. A Critical Look at Multilayered Polymer Capsules in Biomedicine: Drug Carriers, Artificial Organelles, and Cell Mimics. Adv Funct Mater. 2011; 21:14–28.
40. Tu Y, Peng F, Adawy A, Men Y, Abdelmohsen LK, Wilson DA. Mimicking the Cell: Bio-Inspired Functions of Supramolecular Assemblies. Chem Rev. 2015; 116:2023–2078. [PubMed: 26583535]
41. Martino C, Kim SH, Horsfall L, Abbaspourrad A, Rosser SJ, Cooper J, Weitz DA. Protein Expression, Aggregation, and Triggered Release from Polymersomes as Artificial Cell-Like Structures. Angew Chem, Int Ed. 2012; 51:6416–6420.
42. van Dongen SF, Nallani M, Cornelissen JJ, Nolte RJ, van Hest A. Three-Enzyme Cascade Reaction through Positional Assembly of Enzymes in a Polymersome Nanoreactor. Chem - Eur J. 2009; 15:1107–1114. [PubMed: 19072950]
43. Wang M, Alberti K, Sun S, Arellano CL, Xu Q. Combinatorially Designed Lipid-like Nanoparticles for Intracellular Delivery of Cytotoxic Protein for Cancer Therapy. Angew Chem, Int Ed. 2014; 53:2893–2898.
44. de Gracia Lux C, Joshi-Barr S, Nguyen T, Mahmoud E, Schopf E, Fomina N, Almutairi A. Biocompatible Polymeric Nanoparticles Degrade and Release Cargo in Response to Biologically Relevant Levels of Hydrogen Peroxide. J Am Chem Soc. 2012; 134:15758–15764. [PubMed: 22946840]

45. Sullivan SP, Koutsonanos DG, del Pilar Martin M, Lee JW, Zarnitsyn V, Choi SO, Murthy N, Compans RW, Skountzou I, Prausnitz MR. Dissolving Polymer Microneedle Patches for Influenza Vaccination. Nat Med. 2010; 16:915–920. [PubMed: 20639891]

46. Donnelly RF, Singh TRR, Woolfson AD. Microneedle-based Drug Delivery Systems: Microfabrication, Drug Delivery, and Safety. Drug Delivery. 2010; 17:187–207. [PubMed: 20297904]

47. Kim YC, Park JH, Prausnitz MR. Microneedles for Drug and Vaccine Delivery. Adv Drug Delivery Rev. 2012; 64:1547–1568.

48. Prausnitz MR. Microneedles for transdermal drug delivery. Microneedles for Transdermal Drug Delivery. Adv Drug Delivery Rev. 2004; 56:581–587.

49. Bariya SH, Gohel MC, Mehta TA, Sharma OP. Microneedles: an Emerging Transdermal Drug Delivery System. J Pharm Pharmacol. 2012; 64:11–29. [PubMed: 22150668]

50. Yang S, Wu F, Liu J, Fan G, Welsh W, Zhu H, Jin T. Phase-Transition Microneedle Patches for Efficient and Accurate Transdermal Delivery of Insulin. Adv Funct Mater. 2015; 25:4633–4641.

51. Gittard SD, Chen B, Xu H, Ovsianikov A, Chichkov BN, Monteiro-Riviere NA, Narayan RJ. The Effects of Geometry on Skin Penetration and Failure of Polymer Microneedles. J Adhes Sci Technol. 2013; 27:227–243. [PubMed: 23543070]

52. Tai W, Mo R, Di J, Subramanian V, Gu X, Buse JB, Gu Z. Bio-inspired Synthetic Nanovesicles for Glucose-Responsive Release of Insulin. Biomacromolecules. 2014; 15:3495–3502. [PubMed: 25268758]

53. Lu H, Wang J, Bai Y, Lang JW, Liu S, Lin Y, Cheng J. Ionic Polypeptides with Unusual Helical Stability. Nat Commun. 2011; 2:206. [PubMed: 21343924]

54. Wang J, Lu H, Kamat R, Pingali SV, Urban VS, Cheng J, Lin Y. Supramolecular Polymerization from Polypeptide-Grafted Comb Polymers. J Am Chem Soc. 2011; 133:12906–12909. [PubMed: 21761879]

55. Lu Y, Aimetti AA, Langer R, Gu Z. Bioresponsive Materials. Nat Rev Mater. 2016; 1:16075–16092.

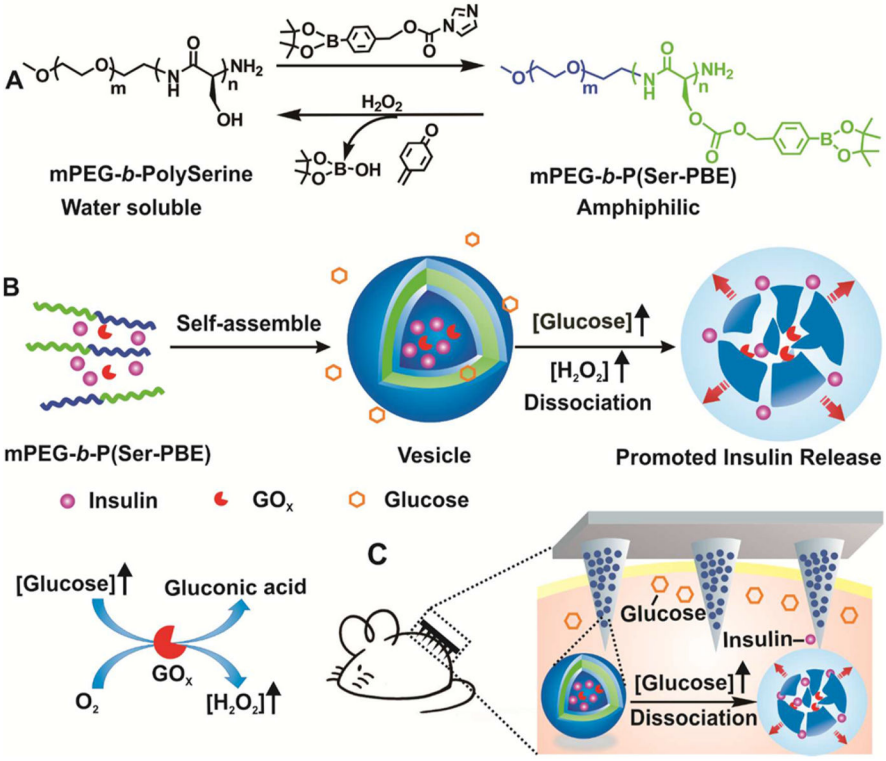


**Figure 1.**

Schematic of the $H_2O_2$-responsive vesicles for glucose-mediated insulin delivery: (A) chemical structure of mPEG-*b*-P(Ser-PBE) and its degradation products; (B) self-assembly of block copolymer mPEG-*b*-P(Ser-PBE) into vesicles loaded with insulin and GOx. The vesicles are dissociated to release insulin in the presence of a hyperglycemic state; (C) PVs were further integrated into the hyaluronic acid (HA)-based microneedle-array patches for smart insulin delivery in a mouse model of type 1 diabetes.

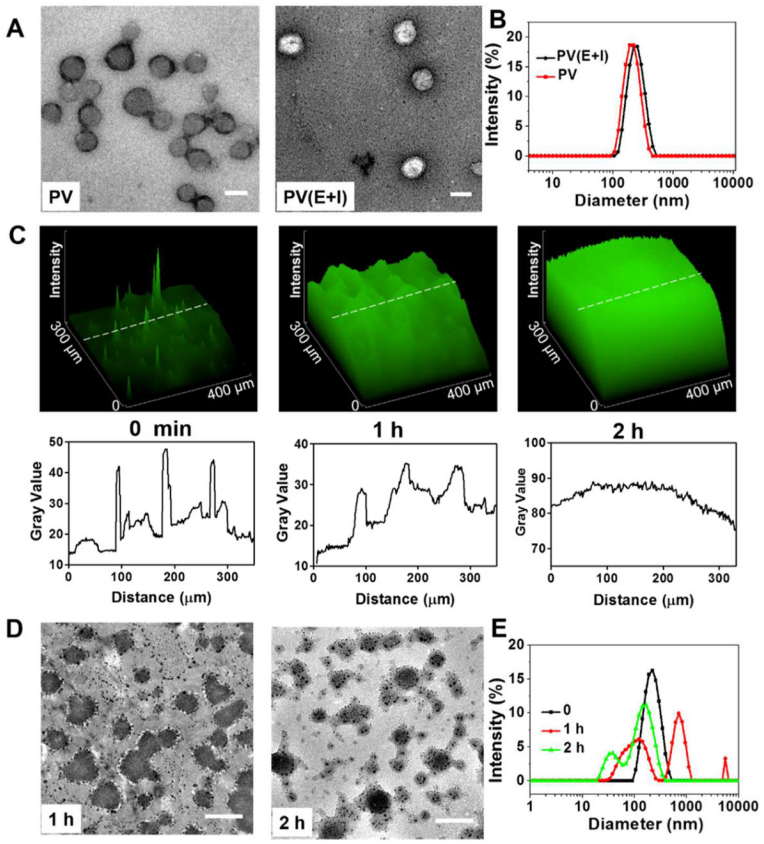


**Figure 2.**

Characterization of glucose-responsive polymer vesicles (PVs). (A) TEM images of (left) blank polymeric vesicles (PVs) and (right) vesicles encapsulated with GOx enzyme and insulin (PVs(E+I)), scale bar is 200 nm; (B) size distribution of PV and PV(E+I). (C) (Top) 2.5D fluorescence images of PV(E+I) solution pre- and postincubation in 400 mg/dL glucose solution for 1 and 2 h at 37 °C, respectively. (Bottom) Distribution of the fluorescence intensity along the indicated white dash line in arbitrary unit (a.u.); (D, E) TEM images (D) and size distribution (E) of PV(E+I) postincubation in 400 mg/dL glucose solution for 1(D, left) and 2 (D, right) h at 37 °C, respectively. Scale bar is 200 nm.

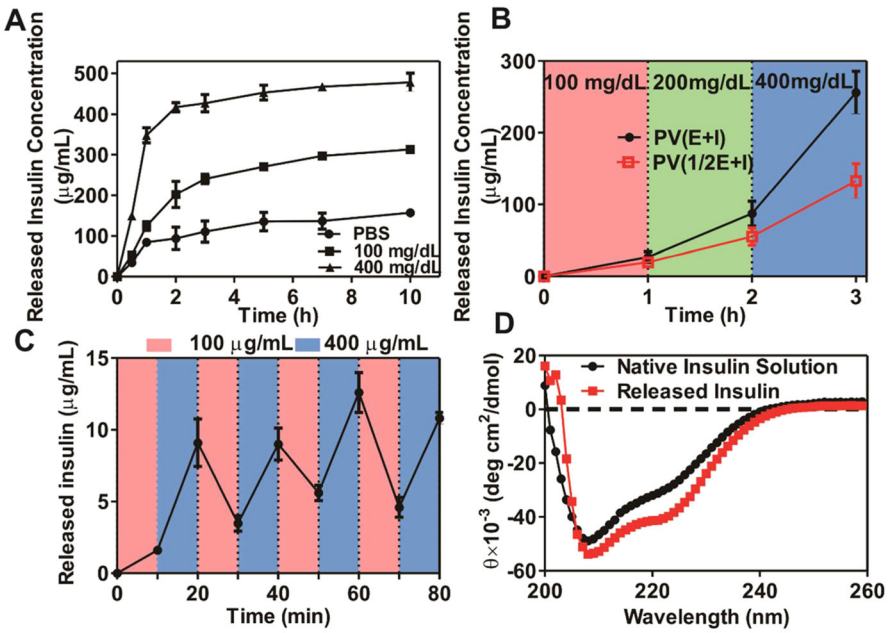


**Figure 3.**

*In vitro* glucose-responsive release of insulin from PVs. (A) *In vitro* released insulin concentration from PVs(E+I) at several glucose concentrations at 37 °C; (B) The release rate (line slope) of insulin as a function of glucose concentration in the release media for PV(E+I) and [PV($^1/_2$E+I) (containing one-half amount of GOx compared to PV(E+I)]; (C) Pulsatile release profile of insulin from PV(E+I) when the glucose concentration changed between 100 and 400 mg/dL alternatively for 10 min each; (D) CD spectra of native insulin solution and insulin released from the PVs incubated with 400 mg/mL glucose. Error bars indicate SD ($n$ = 3).

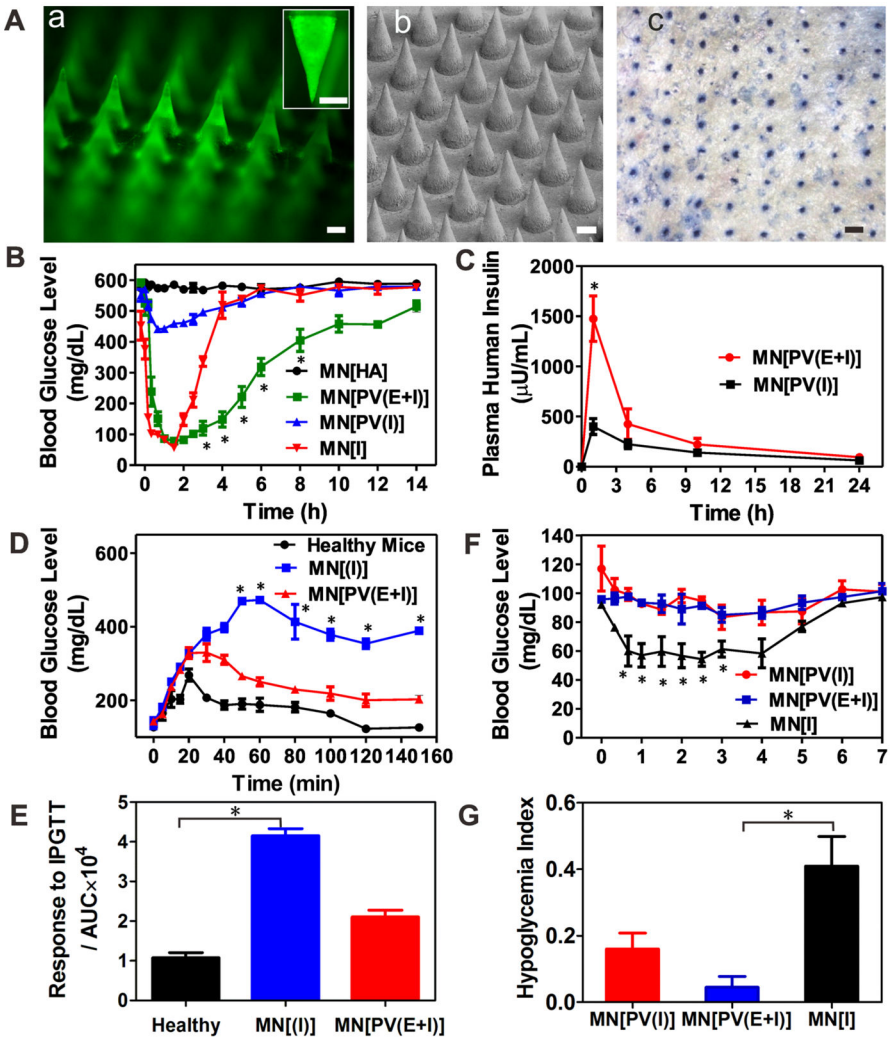


**Figure 4.**

Characterization and *in vivo* studies the MN-array patch for type 1 diabetes treatment. (A)(a) Fluorescence microscopy image of MN loaded with PVs containing FITC-labeled insulin. (Inset is zoomed-in image of MN). Scale bar is 200 $\mu$m. (b) SEM image of an MN patch. Scale bar is 200 $\mu$m. (c) Trypan blue staining of mouse skin transcutaneously treated with an MN-array patch for 1 h. (B) Blood glucose levels in STZ-induced diabetic mice after treatment with MN[HA], MN[I], MN[PV(E+I)], and MN[PV(I)]. *$P < 0.05$ for administration with MN[PV(E+I)] compared with MN[I]. (C) Plasma human insulin concentrations in STZ-induced diabetic mice after treatment with MN[PV(E+I)] and MN[PV(I)]. *$P < 0.05$ for administration with MN[PV(E+I)] compared with MN[PV(I)]. (D) *In vivo* glucose tolerance test toward diabetic mice 1 h post-administration of MN[PV(E+I)] or MN[I] in comparison to the healthy mice. *$P < 0.05$ for administration with MN[PV(E+I)] compared with MN[I]. (E) Responsiveness was calculated based on the area under the curve (AUV) in 150 min, with the baseline set at the 0 min blood glucose reading. *$P < 0.05$ for administration with MN[I] compared with healthy mice. (F) Blood glucose changes of healthy mice treated with MN patch over time. *$P < 0.05$ for administration with

MN[PV(E+I)] compared with MN[I]. (G) Quantification of the hypoglycemia index, which was calculated as the difference between the initial and nadir blood glucose readings divided by the time at which the nadir was reached. *$P < 0.05$ for administration with MN[PV(E+I)] compared with MN[PV(I)]. Error bars indicate SD ($n = 5$).